Modeling energy dependence of the inner-shell x-ray emission produced by femtosecond-pulse laser irradiation of xenon clusters

Timothy C. Berkelbach,* James Colgan, and Joseph Abdallah, Jr.
Theoretical Division, Los Alamos National Laboratory, Los Alamos, New Mexico 87545, USA

Anatoly Ya. Faenov and Tatiana A. Pikuz
Joint Institute for High Temperatures, Russian Academy of Sciences, Moscow 125412, Russia
and Kansai Photon Science Institute, Japan Atomic Energy Agency, Kizu, Kyoto 619-0215, Japan

Yuji Fukuda and Koichi Yamakawa
Kansai Photon Science Institute, Japan Atomic Energy Agency, Kizu, Kyoto 619-0215, Japan
(Received 8 September 2008; revised manuscript received 31 October 2008; published 14 January 2009)

We employ the Los Alamos suite of atomic physics codes to model the inner-shell x-ray emission spectrum of xenon and compare results with those obtained via high-resolution x-ray spectroscopy of xenon clusters irradiated by 30 fs Ti:Sapphire laser pulses. We find that the commonly employed configuration-average approximation breaks down and significant spin-orbit splitting necessitates a detailed level accounting. We reproduce an interesting spectral trend for a series of experimental spectra taken with varying pulse energy for fixed pulse duration. To simulate the experimental measurements at increasing beam energies, we find that spectral modeling requires an increased hot electron fraction, but decreased atomic density and bulk electron temperature. We believe these latter conditions to be a result of partial cluster destruction due to the increased energy in the laser prepulse.

DOI: 10.1103/PhysRevE.79.016407 PACS number(s): 52.50.Jm

I. INTRODUCTION

The use of atomic clusters as sources for ultrashort laser-produced plasmas has been of considerable interest in recent years [1–4]. When high-pressure gas jets are expanded into vacuum, the van der Waals interaction induces clustering with atomic densities approaching that of the solid state. Furthermore, the atomic clusters' intrinsic spatial separation inhibits energy dissipation found in traditional solid-state targets, resulting in very efficient energy absorption. Potential applications include the industrial production of x rays, medicine, and biology, and even nuclear fusion. Because of this, the ability to accurately explain and predict the associated plasma kinetics and spectroscopy is highly desirable.

The lifetime of such laser-produced plasmas is remarkably short and, as such, experimental determination of many important plasma properties is very difficult. Thus, by comparing with an experimental observable such as the emission spectrum, computational modeling both provides a methodology for systematic determination of plasma conditions and helps understand how plasma properties depend on the underlying physics. Previous computational studies employing a variety of atomic- and plasma-physics-based techniques have been very successful in describing and matching experimental results. Such studies have examined the time dependence of plasma properties [5], the plasma expansion [6,7], as well as the influence of gas pressure [8], hot electrons [9,10], and hollow atoms [11].

In this work, we utilize the Los Alamos atomic physics codes—which take the plasma density, electron temperature, and optional hot electron temperature and fraction as input—to model the *L*-shell emission spectrum of Xe. We compare our results with those recently obtained at the Advanced Photon Research Center in Japan via femtosecond-laser-pulse irradiation of Xe clusters. The influence of hot electrons, which are known to be produced in such high-energy laser pulses, as well as a strong prepulse effect, are found to be essential in reproducing the experimental spectra and its energy dependence. Previous studies of Ar clusters produced by ultrashort laser pulses using similar joint theoretical and experimental investigations also explored the effect of hot electrons and other properties of the laser-produced plasma [5,10–14].

In Sec. II we describe the Xe cluster irradiation experiments and present the obtained spectra. Section III contains a description of the theoretical methods used, including the atomic physics and collisional radiative kinetics codes, with an example of the sensitivity of modeled spectra to the level of approximation used. In Sec. IV, we explore the dependence of the modeled spectra on electron temperature, atomic density, and fraction of hot electrons. We compare the modeled spectra to experiment and reproduce an interesting spectral trend obtained for a varying laser pulse energy at fixed duration. In Sec. V, we summarize this work and draw conclusions regarding emission spectra of high-*Z* atomic clusters and the influence of the laser prepulse.

II. EXPERIMENTAL METHOD

The Xe cluster experiments were performed with the JAERI (Kyoto, Japan) 100 TW Ti:sapphire laser system based on the technique of chirped pulse amplification, which was designed to generate 20 fs pulses at a 10 Hz repetition

*Present address: Department of Physics and Department of Chemistry, New York University, New York, NY 10003, USA.

rate and is capable of producing focusing intensity up to 10^{20} W/cm^2 [15,16]. The laser pulses centered at 800 nm were generated at 82.7 MHz by a Ti:sapphire laser oscillator (10 fs). The pulses from the oscillator were stretched to 10 ns, and amplified by a regenerative amplifier and two stages of a multipass amplifier. In this study the amplified pulses were compressed to 30 fs by a vacuum pulse compressor yielding a maximum pulse energy of 360 mJ. In this system, after the regenerative amplifier, the pulses go through two double Pockels cells to reduce the prepulse. The contrast ratio between the main pulse and the prepulse that precedes it by 1 ns is greater than 10^5:1.

In a vacuum target chamber, the measured spot size was 11 μm at $1/e^2$, which was 1.1 times as large as that of the diffraction limit. Approximately 64% of the laser energy was contained in the 11 μm Gaussian spot. These parameters give a focused laser peak intensity of 1.0×10^{19} W/cm^2 with a pulse duration of 30 fs and a pulse energy of 200 mJ.

Xe clusters were produced by expanding high-pressure 2 MPa Xe gas into vacuum through a specially designed pulsed conical nozzle with input and output diameters of 0.5 and 2.0 mm, respectively, and a length of 75 mm. The parameters of this nozzle were calculated using a model developed by Boldarev and co-workers [17–19]. The results of this model have been shown to be consistent with experimentally obtained data [12,20]. In particular, comparisons of the spatial distribution of Ar gas density, measured by interferometry, and the spatial distribution of cluster sizes, measured by light scattering diagnostics, have demonstrated the predictive capability of this code.

Simulations of the nozzle employed in this experiment and x-ray emission analysis of similar experiments suggest the production of a dense cluster medium with clusters approximately 1 μm in size [5,21–23]. In this particular case, the modeling predicted clusters around 0.7 μm [19,20]. Since the rate of cluster decay is primarily determined by the number of atoms in the cluster, the use of large clusters in conjunction with the prepulse reduction techniques ensured a direct interaction between the high-density cluster and the main femtosecond pulse. The laser was then focused about 1.5 mm below the nozzle.

The spatially resolved x-ray spectra were measured using focusing spectrometers with spatial resolution [24]. The spherically bent crystal was placed at a distance of 381.2 μm from the plasma source and was centered at λ=4.05 Å, which corresponds to a Bragg angle of 35.7° for fourth-order reflection of the crystal. X-ray spectra registrations have been done using an Andor x-ray charge-coupled device (CCD), which allowed for a very accurate wavelength calibration and spectrum reproducibility. The spectral wavelengths were measured using chosen He-like Ar lines as a reference. This method allowed the measurement of Xe spectral wavelengths with an accuracy of ~0.001 Å.

Plotted in Fig. 1 are a series of spectra taken for a fixed pulse duration of 30 fs with a varying laser energy. The two main features found in the spectra result from emission from Xe ions involving $3d\rightarrow2p$ transitions. We observe that, although the spectrum intensities do indeed decrease with decreasing beam energy, as would be expected, the relative intensity of shorter-wavelength transitions—between 2.95 and 2.97 Å—-actually increases. This interesting trend will prove to be somewhat counterintuitive following studies made in Sec. IV, but can in fact be reproduced based on justifiable physical conditions, as will be shown.

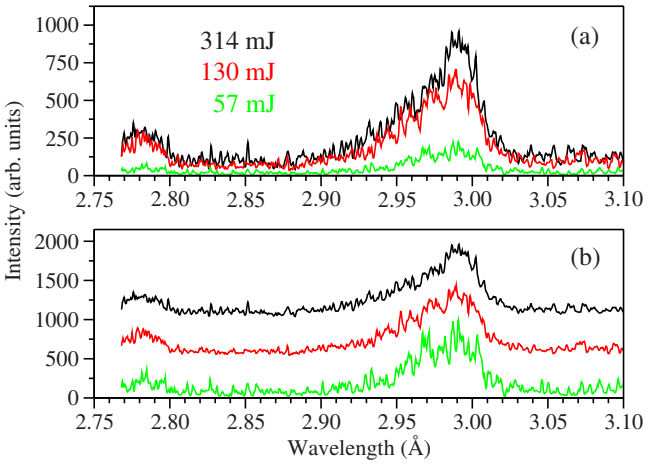

FIG. 1. (Color online) Experimental emission intensities obtained at a pulse length of 30 fs with a varying energy of 314 (top, black), 130 (middle, red), and 57 mJ (bottom, green). The spectra are shown (a) unscaled, to make clear the intensity dependencies, and (b) scaled to a uniform maximum, to portray the spectral dependencies.

III. THEORETICAL METHOD

All calculations were performed using the Los Alamos suite of atomic physics codes: CATS [25], GIPPER [26], and ATOMIC [27]. Atomic structure and collisional excitation cross sections were computed from the CATS code, based on the Hartree-Fock method of Cowan [28]. GIPPER was used for the calculation of collisional ionization cross sections and all data were fed into ATOMIC, which employs a collisional radiative scheme to determine the ion population distribution and subsequent emission spectrum.

Previous studies utilizing configuration-average-based atomic structure energy levels via the unresolved transition array (UTA) or mixed-UTA methods, have succeeded in describing the x-ray emission spectra of lower-Z atoms [11]. The transition of interest in this work, determined to be $3d\rightarrow2p$, undergoes severe spin-orbit splitting due to the high-Z effects of Xe. As such, the L-shell emission spectrum of interest necessitates a detailed level accounting, including approximately 100 000 levels over 2800 configurations in 13 ion stages, from K-like (Xe^{35+}) to Ga-like (Xe^{23+}). Each of the 13 ion stages included configurations from the ground state, single promotion from n=2 to n=(3,4), and double promotion from n=3 to nl=(4s,4p).

Utilization of the configuration-average approximation includes no fine structure via relativistic effects and, as such, includes $3d\rightarrow2p$ transitions for each ion stage, subject to permutations of the spectator electrons. Solution of the full Dirac equation via a Dirac-Fock-Slater procedure results in a so-called relativistic configuration-average description, which includes by nature the spin-orbit interaction, resulting

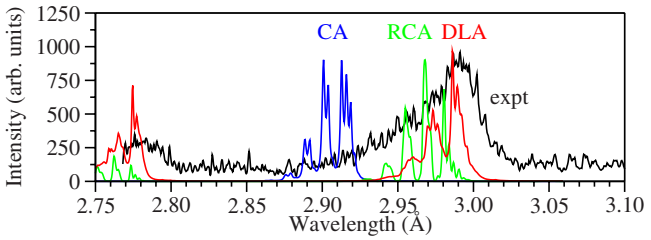

FIG. 2. (Color online) Theoretical emission spectra employing three different approximations: configuration average (CA), relativistic configuration average (RCA), and a detailed level accounting (DLA), all compared to an experimental spectrum. Each calculation was made at an atomic number density of 10^{20} cm^{-3} and an electron temperature of 300 eV.

in a much more accurate spectrum. To feasibly obtain a fine-structure spectrum, we may go one step further and utilize a semirelativistic detailed level accounting (DLA).

This detailed level accounting was achieved through the use of a nonrelativistic Hamiltonian with the usual semirelativistic correction terms:

$$\Delta H = -\frac{1}{2mc^2}(E-V)^2 - \frac{\hbar^2}{4m^2c^2}\left(\frac{dV}{dr}\right)\left(\frac{\partial}{\partial r} - \frac{2}{r}\boldsymbol{l}\cdot\mathbf{s}\right),$$

respectively known as the mass-velocity term, the Darwin term, and the spin-orbit term, in cgs units. The spin-orbit term, which becomes more important for increasing Z, is found to play a most important role, resulting in a prominent splitting effect. To illustrate this, we present in Fig. 2 the experimental spectrum and a series of ATOMIC calculations, each employing a different approximation as indicated, at an electron temperature of 300 eV and an atomic number density of 10^{20} cm^{-3}. The peaks predicted in the configuration-average approximation are in large disagreement with the experimental peaks. Use of a relativistic configuration-average approximation improves things, but clearly the DLA model is closest to the experimental result. The splitting effect found in the DLA (and RCA) calculations is directly due to the spin-orbit interaction term defined previously.

It should be noted that a full fine-structure calculation is far too expensive in this case. Therefore, we follow [29] and solve the kinetics rate equations in the configuration-average approximation, but use DLA to compute the emission spectrum. Here, we have retained DLA for all transition arrays with fewer than 10^6 lines. Furthermore, while our model includes individual detailed levels, there is no configuration-interaction mixing present. Finally, we note that all of the calculations presented here were made assuming steady state, i.e., that the plasma emission spectra are from ions in which the final level populations are reached very quickly, so that no time dependence is present.

IV. RESULTS AND DISCUSSION

In all spectra to follow, spectral lines were modeled as Lorentzians with a width approximately equal to the instrumental resolution, $\Delta\lambda/\lambda = 0.0006$. All reported spectral intensities in Figs. 3–5 are absolute, and in Figs. 6–8 a uniform scaling constant is employed for comparison with experiment.

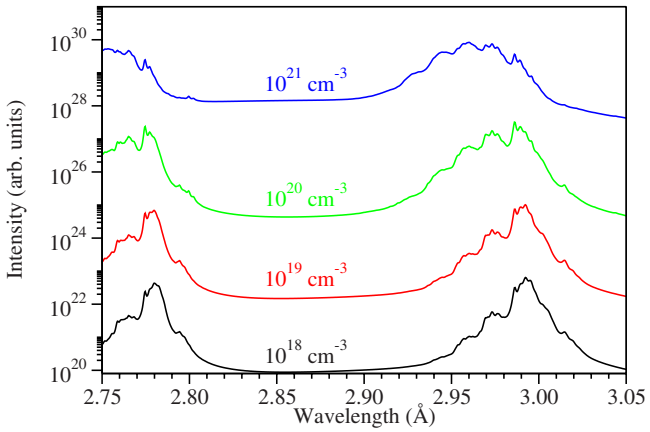

FIG. 3. (Color online) Theoretical emission spectra for varying atomic densities at fixed electron temperature $T_e = 300$ eV.

In an effort to characterize the experimental plasma conditions, we first vary the atomic density N_a at a fixed electron temperature of $T_e = 300$ eV, based on the simulation of a previous experiment with argon clusters [5,30]. Increasing the atom density results in a corresponding increase in electron density, which drives the plasma into a higher ionization state. Figure 3 shows the obtained spectra taken in the range $N_a = 10^{18} - 10^{21}$ cm^{-3}. We see that the spectral features are relatively insensitive to changes in the density until 10^{21} cm^{-3} and beyond, which is approaching solid-state densities, and outside the range of reasonable densities for atomic cluster experiments. Again in agreement with Refs. [5,30], we choose 10^{20} cm^{-3} as an initial guess.

With the atomic density fixed, we now seek the spectral temperature dependence. Plotted in Fig. 4 is a series of emission spectra calculated at $N_a = 10^{20}$ cm^{-3}, with electron temperature $T_e = 200 - 500$ eV. As the electron temperature is increased, the spectrum favors higher-energy transitions. Physically we can understand this trend as follows. Each ion stage of Xe has a localized range of $3d \rightarrow 2p$ transitions occurring at successively shorter wavelengths. As we increase

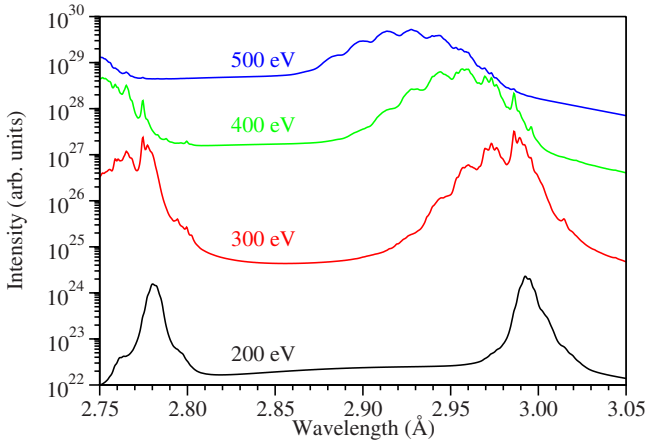

FIG. 4. (Color online) Theoretical emission spectra for varying electron temperatures at fixed atomic density $N_a = 10^{20}$ cm^{-3}.

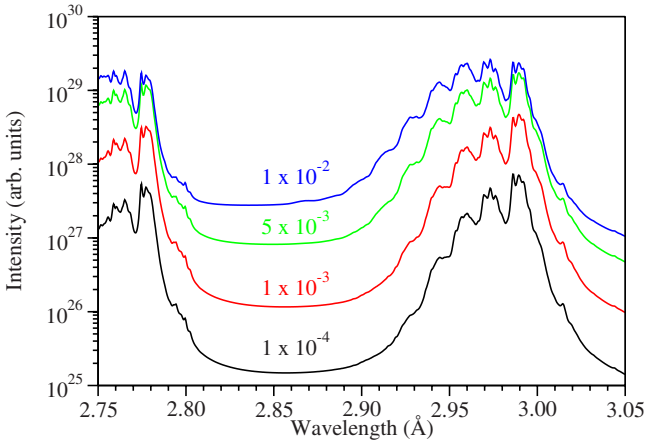

FIG. 5. (Color online) Theoretical emission spectra for varying hot electron fractions at fixed electron temperature $T_e=300$ eV and atomic density $N_a=10^{20}$ cm^{-3}.

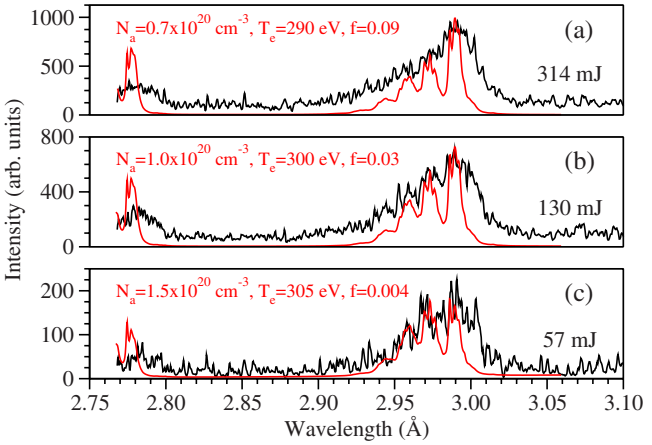

FIG. 7. (Color online) Comparison of spectral features for each laser energy-dependent spectrum (a)–(c). Experimental results are given in black and modeled results in red (gray).

the electron temperature, the ion distribution shifts to greater ionization, thus increasing the intensity of shorter-wavelength spectral lines.

Lastly, we examine the influence of hot electrons. The hot electron temperature was chosen to be $T_{\rm hot}=5$ keV, though previous simulation of Kr clusters have employed a hot electron temperature of 20 keV [31]. Hot electron temperatures as high as 20 keV were explored in our study, with no significant difference in the spectral features. This finding is in good agreement with a generalized study [32] showing that neither the functional form nor the characteristic energy of the hot electrons has a strong influence on the rates as long as the characteristic energy is greater than that of the most energetic transition of interest.

Figure 5 shows a series of spectra taken for a range of hot electron fractions f. Increasing f is observed to be similar to increasing T_e, as could be expected, and substantially increases the spectral intensity. Closer inspection also shows that the spectrum is actually broadened, with transition peaks from a greater range of ion stages, in much better agreement with experiment. This effect is a result of the two-temperature model, which causes a wider, more balanced ion distribution than found in one-temperature models ($f=0$).

We now turn to the problem of matching, and thus diagnosing, the experimental spectra. The problem that presents itself, as has been alluded to in previous sections, is that the lower-energy—and thus lower-intensity—spectra clearly have an increased relative intensity of shorter wavelength (2.95–2.97 Å) transitions. Based on the previous dependency investigations, this trend would intuitively be captured by raising either the electron temperature or the hot electron fraction but this would of course increase the overall intensity as well, in direct opposition to what is seen in experiment, and makes little physical sense.

Thus we seek a physically sensible, variational process that can reproduce high-intensity spectra with decreased relative intensities of shorter-wavelength transitions. The features of the modeled spectra are not independent of one another, and thus a linear-type optimization procedure, where each feature is accurately fixed in succession, is not feasible. Rather, we use a method developed through intuition and experimentation which employs an overshoot-and-correct type of procedure. We first match the mid-intensity spectrum, which is easily found from our results from the previous section, using the physical conditions $N_a=1.0\times10^{20}$ cm^{-3}, $T_e=300$ eV, and $f=0.03$. We then utilize the hot electron fraction to approximate the overall intensities of each spec-

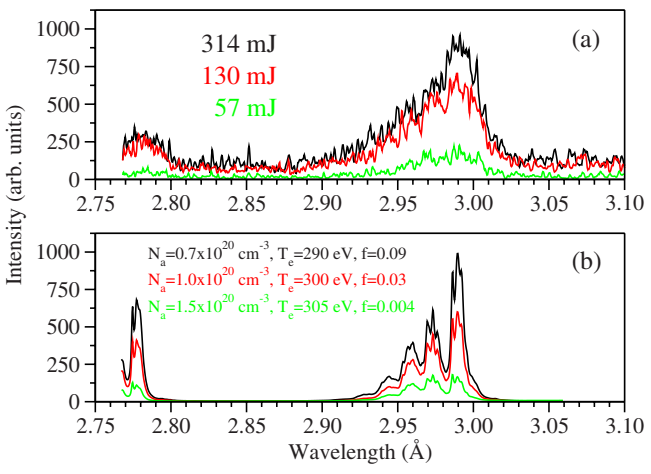

FIG. 6. (Color online) Comparison of relative intensities for experimental spectra (a) with those of the modeled spectra (b).

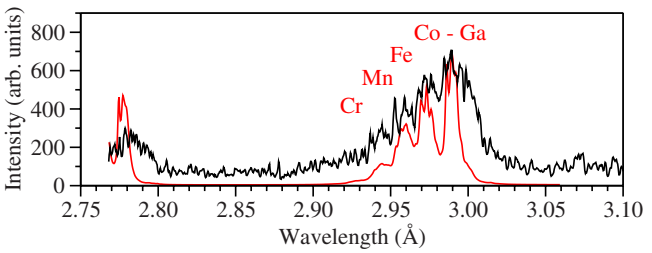

FIG. 8. (Color online) Identification of major peaks for the modeled spectrum [red (gray)] against experiment (black) for the mid-energy, 130 mJ spectrum. Peak wavelength positions for each ion stage are equivalent for all other conditions.

trum in accordance with Fig. 1. With hindsight on our side, we actually overshoot the difference in intensities, i.e., f too high for the high-energy, 314 mJ spectrum (or too low for the low-energy, 57 mJ spectrum) for exact agreement with the relative intensities of Fig. 1. While such an effect could alternatively be achieved through the increase of either electron temperature or atomic density, using the hot electron fraction is advantageous in that it promotes the inclusion of more peaks via a broadening of the ion distribution. Furthermore, we make the assumption that the hot electron fraction will be the parameter most influenced by an increased beam energy for fixed pulse duration and thus must most prominently reflect the appropriate physics.

Although this step does indeed reproduce the correct intensity trend, it misweights the relative intensities of the shorter-wavelength peaks. Thus, our next step is to alter the density in such a way as to correct the relative peak intensities. This procedure of course unfavorably affects the overall intensity as well, but was compensated for via the overshooting of the hot electron fraction. Lastly, we fine-tune the height of the major peak centered around 2.99 Å, which for small changes, can be uniquely adjusted with the bulk electron temperature.

Figures 6 and 7 compare the final results of this procedure with experiment. Figure 6 shows the agreement obtained in reproducing the intensity trend of the experimental spectra. The modeled spectra have of course been left completely unscaled, as required by such a comparison. Figure 7 individually overlays each modeled spectrum with its corresponding experimental spectrum to show the excellent agreement obtained in matching the spectral features, most notably the ratio of peaks between 2.95 and 3.00 Å.

The conditions required to model these experimental trends suggest very interesting physical processes taking place with a strong influence on the spectrum. An increase in hot electron fraction for increasing beam energies is easily understandable in terms of the amount of energy imparted to the cluster in a given length of time. The bulk electron temperature and atomic density dependencies are somewhat more subtle and a little counterintuitive. Usually, as the atomic density decreases, the spectral intensity also decreases, since there are fewer ions to radiate. However, in this case, we find that the spectral intensity increases as the atomic density decreases, due to the increasing fraction of hot electrons included as the atomic density decreases, which is necessary to acceptably match the experimental spectra. This also underscores the importance of hot electrons in this unusual plasma. These trends can be understood physically by analyzing the role of the laser prepulse, which can lead to cluster destruction. We recall that, in the experiments described here, the contrast between the prepulse and main pulse is 10^{-5}, and the prepulse precedes the main pulse by 1 ns. Thus the prepulse has a laser intensity of approximately 10^{13}–10^{14} W/cm^2. It has previously been demonstrated [33,34] that at such intensities multicharged ions of Xe can be formed, which indicates destruction of a significant fraction of the cluster before the interaction of the main pulse. The prepulse for a high-energy beam is thus more likely to cause a premature expansion, by destroying the atomic clusters, and so decreasing the atomic density. Furthermore, we associate this expansion with a cooling of the bulk plasma, resulting in a slight decrease in the electron temperature. In contrast, the lowest-energy beam has a prepulse that minimally affects the integrity of the clusters, which may be modeled by an increased atomic density with slightly hotter electrons. We also note [23] that the intensity of the resulting x-ray spectra will be strongly dependent on the laser contrast.

Our arguments are also qualitatively supported by consideration of the time scales of the cluster dynamics. For a micrometer-sized cluster, as is the case here, the cluster expansion and destruction times are of the order of a few picoseconds [7,35]. This is much shorter than the longer time scale (nanoseconds) prepulse due to amplified spontaneous emission, but of the same order as the prepulse due to residual uncompressed pulse energy (which also has a picosecond time scale). The picosecond prepulse will destroy some fraction of the clusters, causing the expansion. The fraction of the clusters destroyed will be sensitive to the intensity of the prepulse, which is related to the intensity of the main pulse; higher-intensity pulses will have stronger prepulses, leading to great cluster destruction, and so lower bulk atomic densities of the part of the cluster that interacts with the main pulse. The temperature and density conditions used in our modeling then represent the average conditions of the cluster during the peak emission. We note that, even though the cluster expansion is occurring on a picosecond time scale, the spectral emission occurs in a much shorter time, so that consideration of time-dependent dynamics of the electrons is not required.

Finally, we present in Fig. 8 a labeling of the Xe ions which contribute most strongly to each peak in the spectrum. Most notably, our Fe-like peak location is in excellent agreement with the findings of Kondo *et al.* in a previous study of the L- and M-shell emission of Xe [36]. While we could not reproduce a strong theoretical peak just beyond 3.0 Å, as appears to be present in the experimental spectra, there are ion stages with transitions in this region. This experimental peak is believed to be a result of the prepulse, though we could not amplify the intensity of the theoretical peak for any reasonable physical conditions.

V. CONCLUSIONS

To summarize, we have performed accurate plasma modeling for spectral emission from the high-Z element Xe, and have found good agreement with a series of measurements made using high-resolution x-ray spectroscopy of Xe clusters. Inclusion of semirelativistic atomic physics effects, such as spin-orbit splitting, was found to be crucial in order to obtain satisfactory agreement with experiment. Nonrelativistic configuration-average approaches were found to be inadequate for this case. As higher-Z clusters continue to be explored via computational methods, a desire for fine-structure detail will necessitate improved methods for retaining relativistic effects in reasonable times. Nonetheless, our atomic physics calculations were performed at a very high level of theory, utilizing relativistic corrections, and plasma emission

properties were obtained via a configuration-average-based solution of the rate equations with a detailed level accounting for all transition arrays with fewer than 10^6 lines. This procedure results in an emission spectrum with fine-structure detail that matches experimental results quite well.

Additionally, we have presented a procedure for reproducing the spectral trends found in experiment, as the laser energy is increased at fixed pulse duration. An increasing beam energy caused an increase in the hot electron fraction but a decrease in both the atomic density and bulk electron temperature. This latter characteristic is speculated to be a consequence of the experimental prepulse, which partially destroys the cluster before the arrival of the main pulse.

ACKNOWLEDGMENTS

This work was supported under the auspices of the U.S. Department of Energy at Los Alamos National Laboratories under Contract No. DE-AC52-06NA25396. The work was also funded in part by the National Science Foundation through the University of New Mexico/Los Alamos Summer School in Physics. The experimental portion was also supported by the Japan Ministry of Education, Science, Sports and Culture, Grant-in-Aid for Kiban A (20244065), by the RFBR (Projects No. 06-02-16174 and No. 06-02-72005-MNTIa), by ISTC Grant No. 3504, and by the RAS Presidium Program of Basic Research No. 12.

[1] A. McPherson, T. S. Luk, B. D. Thompson, A. B. Borisov, O. B. Shiryaev, X. Chen, K. Boyer, and C. K. Rhodes, Phys. Rev. Lett. **72**, 1810 (1994).
[2] A. McPherson, B. D. Thompson, A. B. Borisov, K. Boyer, and C. K. Rhodes, Nature (London) **370**, 631 (1994).
[3] T. Ditmire, T. Donnelly, A. M. Rubenchik, R. W. Falcone, and M. D. Perry, Phys. Rev. A **53**, 3379 (1996).
[4] T. Ditmire, J. Zweiback, V. P. Yanovsky, T. E. Cowan, G. Hays, and K. B. Wharton, Nature (London) **398**, 489 (1999).
[5] J. Abdallah, Jr. *et al.*, Phys. Rev. A **68**, 063201 (2003).
[6] A. I. Magunov *et al.*, Laser Part. Beams **21**, 73 (2003).
[7] A. Ya. Faenov *et al.*, Laser Part. Beams **26**, 69 (2008).
[8] I. Yu. Skobelev *et al.*, JETP **94**, 966 (2002).
[9] S. B. Hansen *et al.*, Phys. Rev. E **66**, 046412 (2002).
[10] J. Abdallah Jr., A. Ya. Faenov, I. Yu. Skobelev, A. I. Magunov, T. A. Pikuz, T. Auguste, P. D'Oliveira, S. Hulin, and P. Monot, Phys. Rev. A **63**, 032706 (2001).
[11] J. Colgan *et al.*, Laser Part. Beams **26**, 83 (2008).
[12] G. C. Junkel-Vives *et al.*, Phys. Rev. E **65**, 036410 (2002).
[13] G. C. Junkel-Vives, J. Abdallah, Jr., F. Blasco, C. Stenz, F. Salin, A. Ya. Faenov, A. I. Magunov, T. A. Pikuz, and I. Yu. Skobelev, Phys. Rev. A **64**, 021201(R) (2001).
[14] G. C. Junkel-Vives *et al.*, Phys. Rev. A **66**, 033204 (2002).
[15] K. Yamakawa, M. Ayoama, S. Matsuoka, T. Kase, Y. Akahane, and H. Takuma, Opt. Lett. **23**, 1468 (1998).
[16] Y. Akahane, Ma. Jinlong, Y. Fukuda, M. Aoyoma, H. Kiriyama, J. Sheldakoba, A. Kudryashov, and K. Yamakawa, Rev. Sci. Instrum. **77**, 023102 (2006).
[17] A. S. Boldarev *et al.*, JETP Lett. **73**, 514 (2001).
[18] A. S. Boldarev, V. A. Gasilov, and A. Ya. Faenov, Tech. Phys. **49**, 388 (2004).
[19] A. S. Boldarev, V. A. Gasilov, A. Ya. Faenov, Y. Fukuda, and K. Yamakawa, Rev. Sci. Instrum. **77**, 083112 (2006).
[20] F. Dorchies, F. Blasco, T. Caillaud, J. Stevefelt, C. Stenz, A. S. Boldarev, and V. A. Gasilov, Phys. Rev. A **68**, 023201 (2003).
[21] Y. Fukuda *et al.*, JETP Lett. **78**, 115 (2003).
[22] Y. Fukuda *et al.*, Proc. SPIE **5196**, 234 (2004).
[23] Y. Fukuda *et al.*, Laser Part. Beams **22**, 215 (2004).
[24] A. Ya. Faenov, S. A. Pikuz, A. I. Erko, B. A. Bryunetkin, V. M. Dyakin, G. V. Ivanenkov, A. R. Mingaleev, T. A. Pikuz, V. M. Romanova, and T. A. Shelkovenko, Phys. Scr. **50**, 333 (1994).
[25] J. Abdallah, R. E. H. Clark, and R. D. Cowan, Los Alamos National Laboratory Report No. LA 11436-M-I, 1988 (unpublished).
[26] B. J. Archer, R. E. H. Clark, C. J. Fontes, and H. L. Zhang, Los Alamos Report No. LA-UR-02-1526, 2002 (unpublished).
[27] N. H. Magee, J. Abdallah, J. Colgan, P. Hakel, D. P. Kilcrease, S. Mazevet, M. Sherrill, C. J. Fontes, and H. L. Zhang, in *14th APS Topical Conference on Atomic Processes in Plasmas*, edited by J. S. Cohen, S. Mazevet, and D. P. Kilcrease (AIP, Melville, NY, 2004), pp. 168–179.
[28] R. D. Cowan, *The Theory of Atomic Structure and Spectra* (University of California Press, Berkeley, 1981).
[29] S. Mazevet and J. Abdallah, Jr., J. Phys. B **39**, 3419 (2006).
[30] M. Sherrill *et al.*, Phys. Rev. E **73**, 066404 (2006).
[31] S. B. Hansen *et al.*, Phys. Rev. E **71**, 016408 (2005).
[32] S. B. Hansen and A. S. Shlyaptseva, Phys. Rev. E **70**, 036402 (2004).
[33] I. Yu. Skobelev *et al.*, J. Phys. B **32**, 113 (1999).
[34] A. Bartnik, V. M. Dyakin, J. Kostecki, I. Yu. Skobelev, A. Ya. Faenov, H. Fiedorowicz, M. Szczurek, and R. Jarocki, Quantum Electron. **27**, 334 (1997).
[35] Y. Fukuda *et al.*, JETP Lett. **78**, 115 (2003).
[36] K. Kondo, A. B. Borisov, C. Jordan, A. McPherson, W. A. Schroeder, K. Boyer, and C. K. Rhodes, J. Phys. B **30**, 2707 (1997).